Check for updates

Utilization of eggshell waste as green catalyst for application in the synthesis of 1,2,4,5-tetra-substituted imidazole derivatives

Maryam Mahmoudiani Gilan[1] · Ardeshir Khazaei[1] · Negin Sarmasti[1]

Abstract

Eggshell as a solid waste was loaded on a nano-Fe_3O_4 surface. Then, in one step, it (Fe_3O_4@eggshell) was converted to Fe_3O_4@$Ca_3(PO_4)_2$ as a nano-magnetic, green, cheap, and environmentally friendly catalyst. Techniques such as FT-IR, VSM, FESEM, TEM, EDX, XRD, and TGA were used to characterize the as-synthesized catalyst. The catalytic activity of Fe_3O_4@$Ca_3(PO_4)_2$ was evaluated in the synthesis of 1,2,4,5-tetra-substituted imidazole derivatives through a one-pot multicomponent reaction. The design of the experiment as a systematic statistical approach was used to obtain the optimum point of the reaction condition so that 0.05 g of the as-synthesized catalyst and 94.77 °C were the best condition (which provides 90% yield for the benchmark reaction). Then, 1,2,4,5-tetra-substituted imidazole derivatives in the optimum condition were synthesized with very low reaction times in good yields. The as-prepared catalyst was retrieved through a magnet and used several times without significant loss of catalytic activity.

Graphical abstract
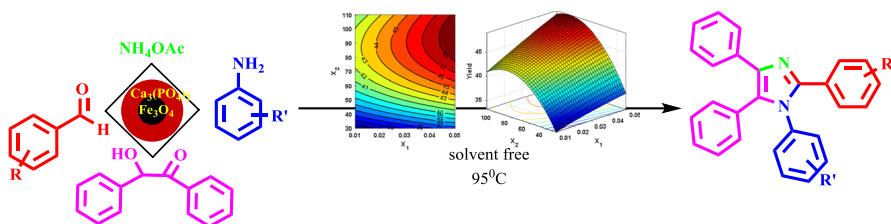
✉ Ardeshir Khazaei
Khazaei_1326@yahoo.com

1 Faculty of Chemistry, Bu-Ali Sina University, Hamedan 6517838683, Iran

🖉 Springer

Introduction

Based on the number of species participating in the reaction, organic reactions can be divided into three categories, namely, one-component reactions, two-component reactions, and one-pot multicomponent reactions (MCRs) [1]. MCRs have attracted keen interest from researchers due to advantages such as atom-economic, effective, eco-friendly, high convergence, reduction of intermediate steps, reducing time and energy, and a high bond-forming-index [2, 3]. Mannich 3CR [4], Strecker 3CR [5, 6], Passerini 3CR [7], Ugi 3CR [8], Pauson–Khand 3CR [9], an Leusen 3CR [10], Gewald 3CR [11], Hantzsch 3CR [12], and Staudinger 3CR [13] are well-known prototypical examples of MCRs. Synthesis of multi-substituted imidazoles is of special importance due to their widespread biological activities [14]. Cimetidine and losartan are among the examples which have entered the drug market. Synthesis of 1,2,4,5-tetra-substituted imidazole (1245-TSI) derivatives through MCR is important due to their biological properties [14]. With respect to the vital role of catalysts in chemical reactions, a large number of catalysts and methods have been used for the synthesis of 1245-TSI derivatives so that solid phase synthesis [15], microwave irradiation [16], sodium benzenesulfinate [17], $ZrCl_4$ [18], molecular iodine [19], $K_5CoW_{12}O_{40} \cdot 3H_2O$ [20], $HClO_4 \cdot SiO_2$ [21], Keggin-type heteropoly-acid (HPA) [22], $InCl_3.3H_2O$ [23], $BF_3 \cdot SiO_2$ [24], $[(CH_2)_4SO_3HMIM][HSO_4]$ [25], $H_6P_2W_{18}O_{62} \cdot 24H_2O$ [26], trifluoroacetic acid (TFA) [27], sulfated zirconia (SZ) [28], silica-bonded propylpiperazine N-sulfamic acid [29, 30], SiO_2-Pr-SO_3H [31], and $Fe_3O_4@SiO_2@TiO_2$ [32] have been used in the synthesis of 1245-TSI. However, most of the cited catalysts are synthesized using pure chemicals. In recent years, some environmental friendly and cheap materials such as eggshells have been used in organic transformations. Calcinated eggshell has been used in biodiesel synthesis [33], hydrogen/syngas, waste water treatment and high-value compounds [34]. In addition, modified eggshell, namely, eggshell/Fe_3O_4 [35], eggshell membrane/noble metal nanoparticles [36], eggshell/Pd [37], Pd-Ag/Al_2O_3 eggshell [38], eggshell/ $Cu(OH)_2$ [39], $Fe_3O_4@Ca(HSO_4)_2$ [40] have been used in organic MCRs. However, most of the cited catalysts are synthesized using pure and expensive chemicals with multistep harsh reaction conditions. With this in mind, in the present work, egg-shells as a waste product (high quantities of this solid residue are still being dis-posed as waste in landfills without any pretreatment) were used for the synthesis of nano-magnetic-$Fe_3O_4@Ca_3(PO_4)_2$ as a green, cheap, environmentally friendly catalyst, and its catalytic activity was evaluated in the synthesis of 1245-TSI deriva-tives as added-value compounds. The results will provide an opportunity to moti-vate researcher interest for further modification of eggshells to be utilized in organic transformations.

Experimental

Materials and apparatus

All chemicals were supplied from Merck and Fluka. The products were character-ized using ^{1}H,^{13}C NMR, melting points as well as IR spectroscopy. The relevant spectral data have been given in the Electronic supplementary information (ESI).[†] The ^{1}H, ^{13}C NMR (250 MHz) was recorded on a Bruker Advance DPX-400 FT-NMR spectrometer (δ in ppm). Melting points were measured using a Büchi B-545 apparatus in open capillary tubes. Perkin Elmer PE-1600-FTIR was used to record the infrared spectra of the products. To measure the mass reduction of the catalyst, thermal gravimetric analysis (TGA) under a nitrogen atmosphere was used. Field-emission scanning electron microscopy (FESEM), and transmission electron microscopy (TEM) images were recorded with SIGMA VP-500 (ZEISS) and Zeiss-EM10C-100 kV, respectively. Elemental analysis of the as-synthesized catalyst was determined using an energy dispersive X-ray analysis (Oxford Instru-ment). A vibrating sample magnetometer (VSM) model (MDKB) was used to determine the saturation magnetization of the catalyst. To monitor the reaction progress, thin layer chromatography (TLC; using silica gel SIL G/UV 254 plates) was used.

Synthesis of the catalyst

Synthesis of Fe_3O_4 nanoparticles

The magnetic (Fe_3O_4) nanoparticles were synthesized by the coprecipitation method [51]. First, 11.3 g $FeCl_3·6H_2O$ and 5.6 g $FeCl_2·4H_2O$ were dissolved in deionized water at 80 °C and 600 rpm. After complete dissolution of the salts, 25 ml ammo-nia (28 wt%) were added en masse to the solution. The resulting black solution was vigorously stirred for 2 h at 80 °C in an N_2 atmosphere. Then, the precipitated mag-netic nanoparticles were separated from the solution using a magnet. Next, the solu-tion was washed several times with water and then with acetone; finally, 10 g stable black magnetic dispersion was obtained and dried in an oven.

Preparation of eggshell powder

Eggshells were collected at home and washed with warm tap water, and then the adhering membrane was separated manually. The eggshells were boiled in distilled water for 2 h and then washed with distilled water. After drying in an oven (120 °C for 2 h), their size was reduced using a cutting mill. Eggshells contain organic impu-rities that should be removed before use so that 100 mL CH_2Cl_2 was added to the powder which was subject to ultrasound for 2 h. Finally, the powder was separated using filtration and dried in an oven.

Preparation of Fe₃O₄@eggshell

An amount of 1 g of the eggshell powder was added to 100 mL of water and stirred for 10 min at room temperature, and then 0.5 g as-synthesized nano-Fe_3O_4 was added to the mixture, which was dispersed for 15 min using ultrasound and stirred for 2 h at 60 °C. There are two kind of intermolecular interactions between Fe_3O_4 and $CaCO_3$, which are electrostatic and electrodynamics, together with electrostatic–electrodynamics, . The intermolecular interactions are strong enough to prevent separation of the eggshell from the Fe_3O_4 which the experimental results confirm. Finally, the nano-Fe_3O_4@eggshell (0.7 g) was filtered and dried in an oven.

Preparation of Fe₃O₄@Ca₃ (PO₄)₂

First, 0.7 g of Fe_3O_4@eggshell powder was dispersed in 50 mL acetone using sonication, and then an extra amount of H_3PO_4 was added dropwise to the suspension. The reaction medium was stirred continuously until all gases were exhausted. In sequence, the acetone was evaporated at 60 °C up to $LOD \approx 0$ (loss on drying). In this step, Fe_3O_4@eggshell was converted to Fe_3O_4@Ca_3 $(PO_4)_2$ (1.1 g).

Results and discussion

Characterization of the catalyst

FT-infrared

This technique is used to identify the functional group on the material/particles and the IR spectra of the Fe_3O_4, eggshell, Fe_3O_4@eggshell, Fe_3O_4@$Ca_3(PO_4)_2$, and $Ca_3(PO_4)_2$ are shown in Fig. 1, in which is shown the IR spectrum of Fe_3O_4@eggshell as a hybrid of Fe_3O_4, and eggshell spectra confirm the loading of eggshell on the Fe_3O_4 core. The $CaCO_3$ is converted to Ca_3 $(PO_4)_2$ [$H_3PO_4 + CaCO_3 \rightarrow Ca_3$ $(PO_4)_2 + H_2O + CO_2$] in the synthesis procedure in which H_3PO_4 is added to the Fe_3O_4@eggshell. Hence, the wave numbers which are related to the $CaCO_3$ must disappear and the wave numbers of Ca_3 $(PO_4)_2$ must appear in the IR spectra. To confirm the formation of Fe_3O_4@Ca_3 $(PO_4)_2$, the IR spectra of Ca_3 $(PO_4)_2$ was recorded, which is shown in Fig. 1. As is clear, the IR spectrum of Fe_3O_4@Ca_3 $(PO_4)_2$ is matched with the IR spectrum of Ca_3 $(PO_4)_2$. Similarities are shown by dotted black rectangles. The IR spectra show the vibration modes of PO_4^{3-} ions at 467, 564, 602, 962, 1036, and 1102 cm^{-1}. The wave numbers of 636 and 3576 cm^{-1} are related to the hydroxyl groups [41].
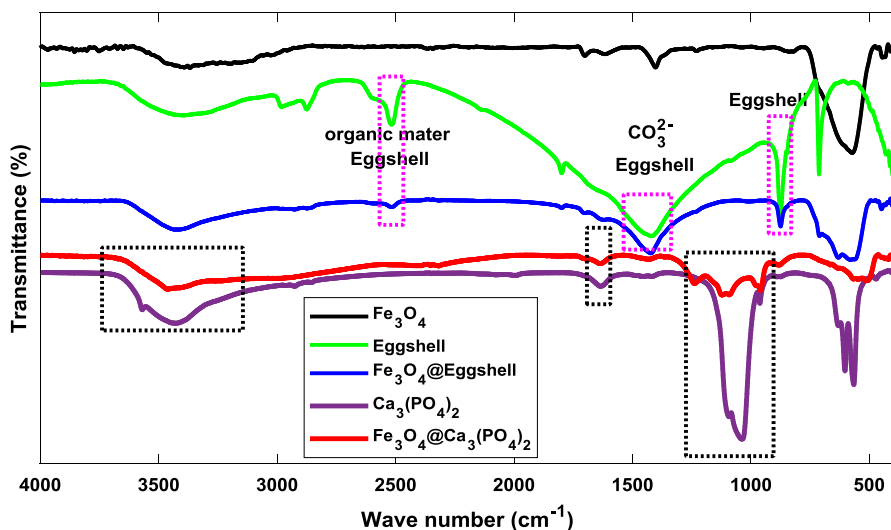
Fig. 1 FT-IR spectra of Fe_3O_4, eggshell, Fe_3O_4@eggshell, Fe_3O_4@$Ca_3(PO_4)_2$, and $Ca_3(PO_4)_2$

Vibrating sample magnetometer

This technique is used to investigate the magnetization property of a material. The VSM of the as-synthesized Fe_3O_4 and the final catalyst, namely Fe_3O_4@$Ca_3(PO_4)_2$, are shown in Fig. 2. The degree of saturation magnetization of Fe_3O_4 decreases from 54 to 14.58 emu/g in the final catalyst (Fe_3O_4@$Ca_3(PO_4)_2$). Reduced saturation magnetization in Fe_3O_4@$Ca_3(PO_4)_2$ is attributed to the nano-magnetic layer ($Ca_3(PO_4)_2$) in the core/shell structure of the as-synthesized catalyst. Non-magnetic materials quench the surface moment, which in turn decreases saturation magnetization. Although the saturation magnetization is reduced, the
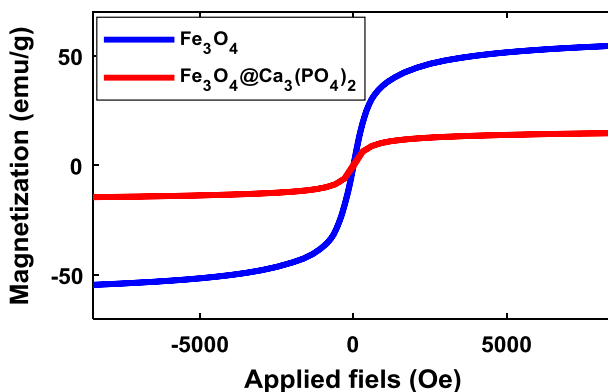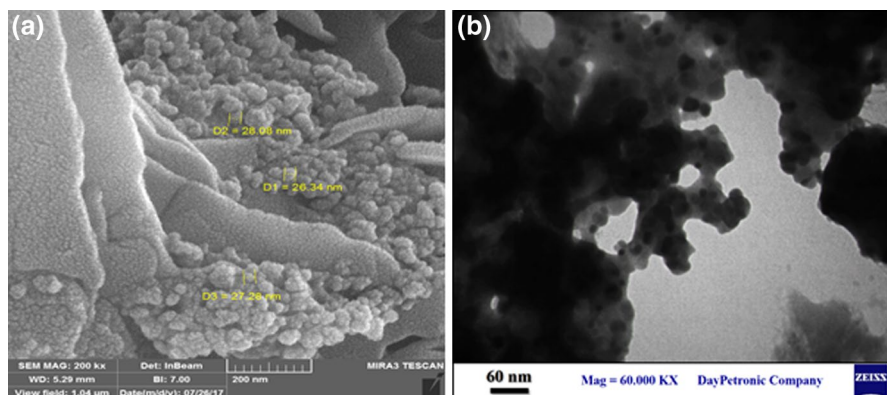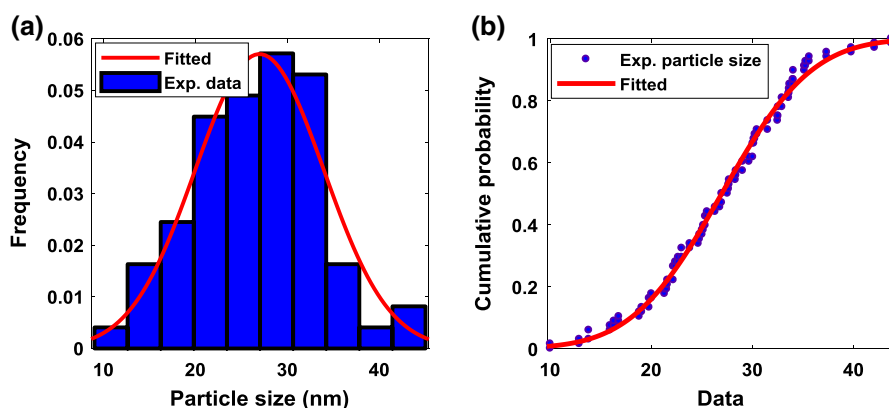

Fig. 2 Magnetization curve of the nano-Fe_3O_4, and nano-Fe_3O_4@$Ca_3(PO_4)_2$

Fig. 3 **a** SEM (*left*) and **b** TEM (*right*) images of the as-synthesized catlayst (Fe$_3$O$_4$@Ca$_3$(PO$_4$)$_2$)

Fig. 4 **a** Normal distribution and **b** cumulative distribution functions of the normal distribution of the as-synthesized catalyst (Fe$_3$O$_4$@Ca$_3$(PO$_4$)$_2$)

as-synthesized catalyst can be easily separated from the reaction mixture and used for the next cycles.

Field-emission scanning electron microscopy and transmission electron microscopy

These techniques are used to identify the size, shape, and morphology of the particles. The FESEM and TEM of the as-synthesized catalyst are shown in Fig. 3. FESEAM (Fig. 3a) shows that the catalyst shape is spherical, but the SEM (Fig. 3b) shows that Fe3O4 nano-particles are coated with a layer of Ca$_3$(PO$_4$)$_2$ which is obtained through the reaction of CaCO$_3$ with H$_3$PO$_4$. In addition, the particle size of the as-synthesized catalyst is shown in Fig. 4. Figure 4a shows the distribution of particle size together with the well-fitted normal distribution function to these data.

Mean and standard deviation of the particles size are 27 nm and 7 nm, respectively. Figure 4b shows the experimental and fitted cumulative distribution functions of the normal distribution, while Fig. 3 shows that 67%, and 90% of the particles size are less than 30 nm and 40 nm, respectively.

Energy-dispersive X-ray spectroscopy (EDX)

This technique is used to determine the approximate contribution of each element of the sample. The EDX pattern (elemental analysis) of the as-synthesized catalyst is given in Fig. 5. The mass percent of the C, O, P, Ca, and Fe are 17.92, 45.71, 22.07, 560, and 8.70, respectively. The elemental analysis of the as-prepared catalyst confirms the formation of $Fe_3O_4@Ca_3(PO_4)_2$ as the final catalyst.

X-ray diffraction (XRD)

This technique is used to identify size, purity, and crystalline nature of the particles. The XRD patterns of Fe_3O_4, Fe_3O_4@eggshell, and $Fe_3O_4@Ca_3(PO_4)_2$ are shown in Fig. 6. XRD patterns together with Scherrer equation $[D=(K\lambda)/(\beta\cos\theta)]$ are used to calculate the particle size of the as-synthesized catalyst. K, λ, β, and θ stand for the dimensionless shape factor, X-ray wavelength, full width at half maximum (FWHM) of the diffraction peak, and Bragg diffraction angle in radian, respectively. It can be assumed that the nanoparticles have a spherical shape so the dimensionless shape factor was set to 0.9. For the X-ray wavelength, copper K-Alpha (λ), namely 0.154184 nm, was used which is the averaged value of $\lambda_{K\alpha1}=0.1540598$ nm, and $\lambda_{K\alpha2}=0.154433$ nm. The XRD pattern gives the values of β and θ. The values of 2θ, FWHM, and the particle size of the as-synthesized catalyst are given in Table 1. The averaged value of the nano-particle size based on the XRD technique is 9.73 nm, which is inconsistent with the result of FESEM (27 nm). This difference can be
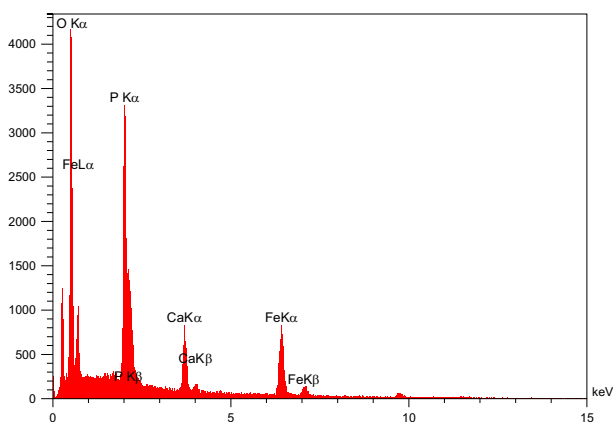
Fig. 5 The elemental analysis of as-synthesized catalyst ($Fe_3O_4@Ca_3(PO_4)_2$) using energy-dispersive X-ray spectroscopy
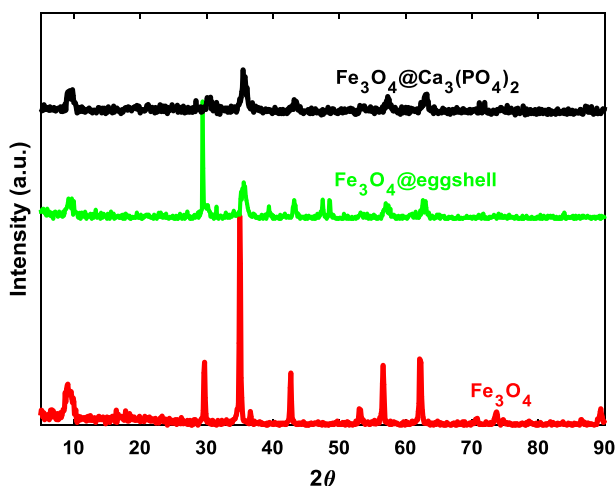
**Fig. 6** XRD pattern of nano-Fe_3O_4, nano-Fe_3O_4@eggshell, and nano-Fe_3O_4@$Ca_3(PO_4)_2$

Table 1 X-ray diffraction (XRD) data for the as synthesized catalyst (Fe_3O_4@$Ca_3(PO_4)_2$)

Entry	2θ	Peak width (FWHM) (radian)	Size (nm)	Interplanar spacing of the crystal (nm)
1	9.38	1.038	7.66	0.94
2	30.38	0.732	10.86	0.29
3	35.68	0.680	11.69	0.25
4	43.35	1.178	6.75	0.21
5	57.31	0.662	12.01	0.16
6	63.13	0.847	9.39	0.15
Mean	–	–	9.73	0.33

explained by the inability to measure smaller particles in the FESEM images, and the *K* value in the Scherrer's equation. The Bragg equation ($d_{hkl} = \lambda/2\sin\theta$) was used to calculate the distance between the layer (*d*-spacing or interplaner spacing) in the crystalline structure of as-synthesized catalyst, and the results are given in Table 1.

Thermal gravimetric analysis and differential thermal analysis (DTA)

Thermal stability of catalyst is a key factor which influences the catalytic activity, and the TGA of the as-prepared catalyst is shown in Fig. 7. The first mass loss up to 105 °C is attributed to the release of adsorbed water. The second loss, from 105 up to 510 °C, can be attributed to the residue of the eggshell organic matters. The mass loss above 510 °C might be related to the loss of CO_2 from the unreacted $CaCO_3$. In addition, differential thermal analysis (DTA) (Fig. 7) confirms the steps of the as-synthesized catalyst weight loss. Figure 7 shows that the as-synthesized catalyst is stable and can be used in high-temperature organic reactions.
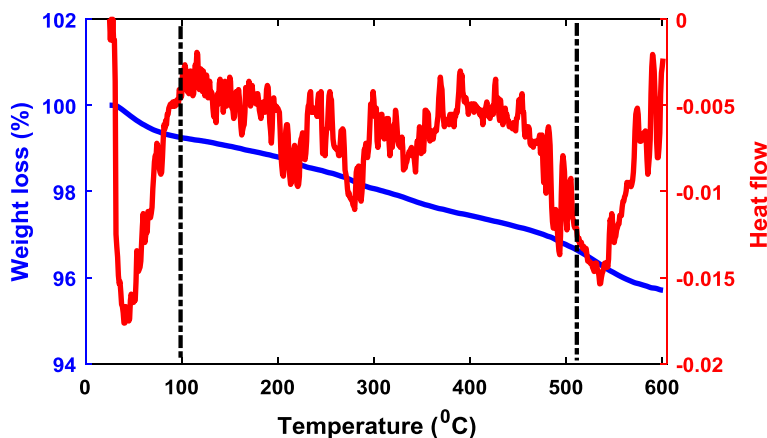
Fig. 7 Thermal gravimetric analysis and differential thermal analysis of the as-synthesized catalyst $Fe_3O_4@Ca_3(PO_4)_2$

BET and BJH analysis

The BET and BJH techniques are used to characterize the surface and pores of a solid material. Accordingly, the surface area, cavity volume and cavity diameter are 1.355×10^5 cm^2/g, 0.02 cm^3/g and 2.26 nm, respectively, for the as-synthesized catalyst.

Evaluation of the catalytic activity of nano-$Fe_3O_4@Ca_3(PO_4)_2$

Effect of solvent type on the reaction

Solvents play an important role in chemical reactivity so that the rate of a reaction may change by orders of magnitude when the solvent is changed. The solvent effects are explained by the interaction of a solvent with the reactants and the transition state of the reaction [42]. Considering this issue, the kinetic effect of different solvents, namely ethyl acetate (EtOAc), acetonitrile (CH_3CN), water, n-hexane, and ethanol (EtOH), were investigated. Using these solvents, the time and reaction yields of the benchmark reactions are given in Table 2. The kinetic effect of the solvents can be explained by the dipole moment of the solvents, which are given in Table 2. By increasing the dipole moment, the reaction yield decreases, which can be attributed to the change of the Gibbs free energy of the reactant and the transition state. On the other hand, the reaction was carried out in a solvent-free condition so that the maximum yield was achieved in a short time. A reduced reaction yield in a solvent is related to the cage effect of the solvent [43], which reduces the mobility of the reactant, which in turn hinders reacting solutes from getting to each other in a solution.

Table 2 Effect of solvent type and solvent-free condition on the reaction yield

Entry	Solvent	Time (min)	Yield[a] (%)	Dipole moment (Debye)
5	n-Hexane	70	35	0
6	EtOH	80	30	1.69
2	EtOAc	75	25	1.78
4	H_2O	> 100	–	1.85
3	CH_3CN	> 100	–	3.3

[a]Isolated yield

Optimization of reaction conditions

Optimization of the reaction operating conditions from the reaction time and yield point of view is highly important in organic synthesis. The conventional method is a one-factor-at-a-time which is currently used by many chemists. This method suffers from the disadvantages of a large number of experiments and a failure to find the correct optimal point [44–46]. To overcome these shortcomings, the design of experiment (DOE) has been developed and is used as a multivariate statistical approach. Response surface methods (RSM) are the most efficient and well-known DOE approach used by researchers. Among the RSM methods, the central composite design (CCD) and Box–Behnken design (BBD) are the two reliable methods [47]. In this work, the CCD method was used to design the required experimental points which must be carried out in the laboratory.

Briefly, amounts of the as-synthesized catalyst and temperature were used as the two main factors affecting the reaction yield at a specified time. From now on, the amount of catalyst, temperature, and reaction yield are shown with X_1, X_2, and Y. The experimental points which must be carried out are given in Table 3. X_1 and X_2 can be shown in a coded scale so that the maximum and minimum level of a variable is shown by $+1$, and -1, respectively. The benchmark reaction (1 mmol benzaldehyde derivtives + 1 mmol aniline + 1 mmol benzyl, and 1.2 mmol ammonium acetate) was carried out in the conditions given in Table 3 and ceased after 15 min. The product was purified through crystallization at room temperature. The crystallization yield of the reactions is given in Table 3.

Optimum reaction condition

To find the optimum reaction condition, it is necessary to establish a relationship between the independent (X) and dependent variables (Y). From a mathematical point of view, this can be achieved through Talyor expansion as follows:

$$Y = \beta_0 + \beta_1 X_1 + \beta_2 X_2 + \beta_{12} X_1 X_2 + \beta_{11} X_1^2 + \beta_{22} X_2^2 + \varepsilon \tag{1}$$

Table 3 The designed experimental points by the BBD method, and the obtained benchmark reaction yields

Runs	Effective variable				Response
	X_1 (amount of catalyst)		X_2 (temperature)		
	Coded levels	Actual levels	Coded levels	Actual levels	Yield
1	0	0.03	1	110.00	46
2	0	0.03	0	70.00	44
3	−1	0.01	0	70.00	43
4	−1	0.01	−1	30.00	33
5	1	0.05	1	110.00	48
6	1	0.05	0	70.00	47
7	0	0.03	−1	30.00	35
8	0	0.03	0	70.00	45
9	−1	0.01	1	110.00	40
10	0	0.03	0	70.00	44
11	1	0.05	−1	30.00	37

where β, X, Y, and ε stand for coefficient, independent, dependent variable, and residue of yield between experimental and the model, respectively. Equation (1) can be shown in matrix notation as follows:

$$Y = \beta X + \varepsilon \quad (2)$$

The method of least squares approach can be used to find the best value of coefficients, as follows:

$$\beta = \left(X^{\mathrm{T}}X\right)^{-1}X^{\mathrm{T}}Y \quad (3)$$

The final obtained equation, which relates the amount of the catalyst and the temperature to the reaction yield, is as follows:

$$Y(\text{yield}) = 19.95 + 77.41X_1 + 0.50X_2 + 1.25X_1X_2 - 526.32X_1^2 - 0.003X_1^2 \quad (4)$$

To show the reliability of the model [Eq. (4)], analysis of variance (ANOVA) was carried out, as given in Table 4. The probability value (p value) of the model rejection is 0.0003, namely 3 in 3000, which shows that the model is reliable and significant from the statistical point of view. The p value of the X_1^2 term is 0.7532, which should be cancelled out from the model, but the model is significant and can be used for further analysis. The coefficient of determination, denoted as R^2, shows how much the model is fitted to laboratory data. The value of 0.98 implies that the model is well-fitted to the data. It should be noted that the high R^2 values do not indicate the ability of the model to predict the reaction yield in the new laboratory conditions. To evaluate the predictive power of the model, an experimental data point in Table 5 was removed and then the model was obtained from the 10 remaining data points. Next, using the removed experimental data point, the yield was calculated

Table 4 Analysis of variance (ANOVA) of the obtained model for the yield versus amount of catalyst and temperature

Source	Probability value (p value)
Model (yield)	0.0003
X_1	0.0013
X_2	<0.0001
X_1X_2	0.1042
X_1^2	0.7532
X_2^2	0.0007
R^2	0.9800
Predicted R^2	0.8374
Lack of fit	0.1900

Table 5 Reaction time and yield with and without catalyst in optimum reaction conditions

	Variables		Response	
	X_1	X_2	Time (min)	Yield (%)
With catalyst	0.032	95	46	90
Without catalyst	–	95	80	45
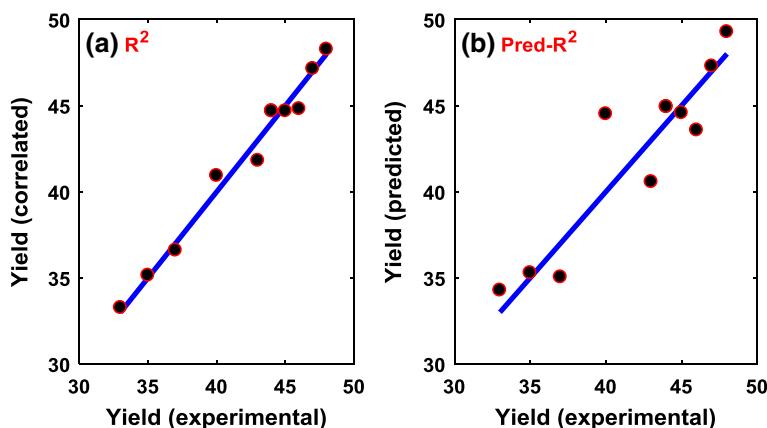
Fig. 8 R^2 and predicted R^2 of the reaction yield by the obtained model

from the obtained model and compared with the experimental reaction yield. This procedure was looped over all the data points, and the Pred_R^2 was calculated. In fact, R^2 and Pred_R^2 show the correlative and predictive power of the model, respectively, as shown in Fig. 8.

Figure 9 shows the 2-dimensional contours and 3-dimentional surface of the reaction yield versus the amount of catalyst (X_1), and temperature (X_2). As is shown, the reaction yield increases as the catalyst increases, but, with increasing temperature,
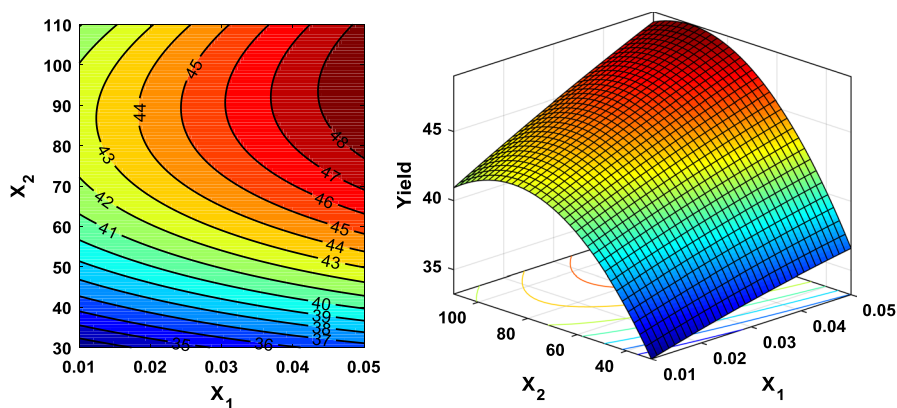
Fig. 9 3-Dimensional surface (*right*) and the 2-dimentional contours (*left*) of the reaction yield versus the amount of catalyst and temperature
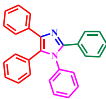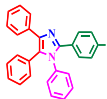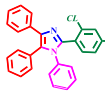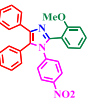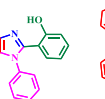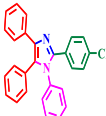
the reaction yield first increases and then decreases. The efficiency has dropped at high temperatures although the effect is not noticeable. This behavior can be explained by the result of the TGA analysis.
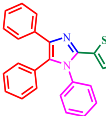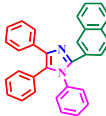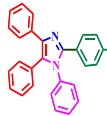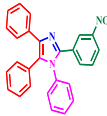
To find the optimum reaction conditions using the constrained value of the amount of catalyst ($0.01 \leq X_1 \leq 0.05$), and temperature ($30 \leq X_2 \leq 110$), the fmincon algorithm in the MATLAB software was used so that 0.05 g and 94.77 °C were obtained for the amount of the catalyst and temperature, respectively. The optimum value of the reaction yield is 48.95 at the specified reaction time (15 min). To investigate the effect of the catalyst on the reaction time and yield, the benchmark reaction was carried out in the optimum conditions with and without the catalyst, and the results are given in Table 5. Using the catalyst, the reaction time and yield are 46 min and 90%, respectively, while, without the catalyst, 45% yield has been obtained in 80 min. These results show that the catalyst has a vital role in the reaction progress.

Synthesis of 1,2,4,5-tetra-substituted imidazole derivatives at optimum reaction condition

It is possible that the optimum reaction conditions for the synthesis of different derivatives have slight differences. However, the obtained optimum conditions for the benchmark reaction were used as generalized conditions in the synthesis of all the derivatives. At the optimum reaction condition (100 °C, and 0.035 g catalyst), 1 mmol benzaldehyde derivatives + 1 mmol aniline + 1 mmol benzyl, and 1.2 mmol ammonium acetate were stirred using a magnet. The reaction progress was monitored using TLC, so that, after completion of the reaction, hot ethanol was added to the reaction media and the catalyst was separated using a magnet. Finally, fine products were obtained through crystallization in the ethanol. The synthesized products together with their melting point, yield, and reaction time are given in Table 6. As is shown, benzene (including electron-withdrawing and electron-donating functional groups) has been successfully

Table 6 Synthesized 1,2,4,5-tetra-substituted imidazole derivatives using the as-synthesized catalyst in optimum reaction conditions

Product	1	2	3	4	5	6
m.p.[a]	219–221	229–232	159–164	210–212	251–253.6	195–198.5
Yield	90	75	65	83	87	92
Time[b]	46	36	75	40	35	25

| Product	7	8	9	10	11
m.p.[a]	187–190	246–248.9	218–220.2	224–226.6	247.1–248.3
Yield	81	75	85	74	82
Time[b]	30	45	30	50	60

[a]Melting point

[b]Time (min)

used with high yield and short reaction times. One of the advantages of the as-prepared catalyst is that the reaction times are very short (in the order of 25–75 min) compared with those reported in the literature (in the order of hours) [23, 28, 31]. On the other hand, phosphate-based catalysts such as potassium phosphate [48], Zr(KPO$_4$)$_2$ [49], and mesoporous zirconium phosphate [50]^2 have been reported, which confirm the utility of the as-prepared catalyst.

Retrieval of the catalyst

In another study, the loss of catalyst activity in different cycles was investigated. After separation of the as-synthesized catalyst using a magnet, the catalyst was washed with ethanol and dried in an oven. The recycled catalyst used in the next cycle and the procedure was repeated for 4 cycles without any reduction in the reaction yield. To cancel out the reaction time, all the cycles were stopped after 40 min. Then, the catalyst was separated with a super-magnet. The resulting solution without any work-up was used for crystallization of the product. The catalyst was dried in an oven for utilizeing in the next cycle. Figure 10 shows the reaction yield versus the number of cycles.

Fig. 10 Benchmark reaction yield versus number of cycles
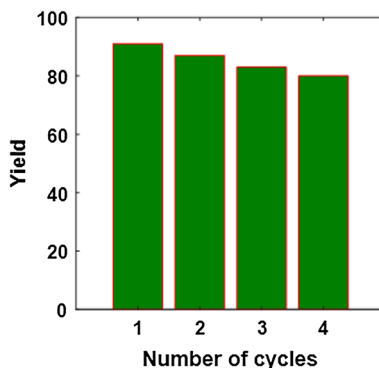
Conclusion

Based on the developed method, eggshells can be used as solid waste in the synthesis of catalysts for use in organic synthesis. The short reaction time and good yields show that the as-prepared catalyst (nano-$Fe_3O_4@Ca_3(PO_4)_2$) has a good catalytic activity in the one-pot synthesis of 1,2,4,5-tetra-substituted imidazole derivatives. Thermal gravimetric analysis showed that the nano-$Fe_3O_4@Ca_3(PO_4)_2$ has a good thermal stability. The design of experiment was used as an efficient approach to find the optimal reaction conditions, and 0.05 g of the catalyst and 94.77 °C were the best conditions found in the current work. It is hoped that this work will motivate researcher interest for further investigations in order to widen the possible conversion of this waste into green and environment-friendly catalysts.

References

1. T. Zarganes-Tzitzikas, A.L. Chandgude, A. Dömling, Chem. Rec. **15**, 5 (2015)
2. L.F. Tietze, Chem. Rev. **96**, 1 (1996)
3. S. Brauch, S.S. van Berkel, B. Westermann, Chem. Soc. Rev. **42**, 12 (2013)
4. C. Mannich, W. Krösche, Arch. Pharm. **250**, 1 (1912)
5. A. Strecker, J. Liebigs, Ann. Chem. **75**, 1 (1850)
6. J.T. Kuethe, D.R. Gauthier, G.L. Beutner, N. Yasuda, J. Org. Chem. **72**, 19 (2007)
7. M. Passerini, L. Simone, Gazz. Chim. Ital. **51**, 126 (1921)
8. I. Ugi, Angew. Chem. Int. Ed. **1**, 1 (1962)
9. P.L. Pauson, I.U. Khand, Ann. N.Y. Acad. Sci. **295**, 1 (1977)
10. A.M. Van Leusen, J. Wildeman, O.H. Oldenziel, J. Org. Chem. **42**, 7 (1977)
11. K. Gewald, E. Schinke, H. Böttcher, Chem. Ber. **99**, 1 (1966)
12. A. Hantzsch, Ber. Deutsch. Chem. Gesellsch. **14**, 2 (1881)
13. H. Staudinger, J. Liebigs, Ann. Chem. **356**, 1 (1907)
14. Y.-B. Nie, L. Wang, M.-W. Ding, J. Org. Chem. **77**, 1 (2012)

15. H.B. Lee, S. Balasubramanian, Org. Lett. **2**, 3 (2000)
16. S. Balalaie, M.M. Hashemi, M. Akhbari, Tetrahedron Lett. **44**, 8 (2003)
17. W. Li, Y. Lam, J. Comb. Chem. **7**, 5 (2005)
18. G.V.M. Sharma, Y. Jyothi, P.S. Lakshmi, Synth. Commun. **36**, 20 (2006)
19. M. Kidwai, P. Mothsra, Tetrahedron Lett. **47**, 29 (2006)
20. L. Nagarapu, S. Apuri, S. Kantevari, J. Mol. Catal. A **266**, 1 (2007)
21. S. Kantevari, S.V.N. Vuppalapati, D.O. Birada, L. Nagarapu, J. Mol. Catal. A **266**, 1 (2007)
22. M.M. Heravi, F. Derikvand, F.F. Bamoharram, J. Mol. Catal. A **263**, 1 (2007)
23. S. Das Sharma, P. Hazarika, D. Konwar, Tetrahedron Lett. **49**, 14 (2008)
24. B. Sadeghi, B.B.F. Mirjalili, M.M. Hashemi, Tetrahedron Lett. **49**, 16 (2008)
25. A. Davoodnia, M.M. Heravi, Z. Safavi-Rad, N. Tavakoli-Hoseini, Synth. Commun. **40**, 17 (2010)
26. A.R. Karimi, Z. Alimohammadi, M.M. Amini, Mol. Divers. **14**, 4 (2010)
27. M.R. Mohammadizadeh, A. Hasaninejad, M. Bahramzadeh, Synth. Commun. **39**, 18 (2009)
28. A. Teimouri, A.N. Chermahini, J. Mol. Catal. A **346**, 1 (2011)
29. K. Niknam, A. Deris, F. Naeimi, F. Majleci, Tetrahedron Lett. **52**, 36 (2011)
30. M.A. Zolfigol, S. Baghery, A.R. Moosavi-Zare, S.M. Vahdat, RSC Adv. **5**, 42 (2015)
31. G. Mohammadi Ziarani, Z. Dashtianeh, M. Shakiba Nahad, A. Badiei, Arab. J. Chem. **8**, 5 (2015)
32. A. Khazaei, A.R. Moosavi-Zare, F. Gholami, V. Khakyzadeh, Appl. Organomet. Chem. **30**, 8 (2016)
33. Y.C. Sharma, B. Singh, J. Korstad, Energy Fuels **24**, 5 (2010)
34. A. Laca, A. Laca, M. Díaz, J. Environ. Manag. **197**, 351 (2017)
35. E. Mosaddegh, F.A. Hosseininasab, A. Hassankhani, RSC Adv. **5**, 129 (2015)
36. R. Mallampati, S. Valiyaveettil, ACS Sustain. Chem. Eng. **2**, 4 (2014)
37. M. Khazaei, A. Khazaei, M. Nasrollahzadeh, M.R. Tahsili, Tetrahedron **73**, 38 (2017)
38. M. Kuhn, M. Lucas, P. Claus, Ind. Eng. Chem. Res. **54**, 26 (2015)
39. E. Mosaddegh, A. Hassankhani, H. Karimi-Maleh, Mater. Sci. Eng. C. **46**, 264 (2015)
40. A. Khazaei, N. Sarmasti, J.Y. Seyf, Appl. Organomet. Chem. **32**, 4 (2018)
41. E. Nordic-Baltic, Conference on biomedical, P. medical, ed. by A. Katashev, Y. Dekhtyar, J. Spigulis, in *M. Intern. Fed. for, E. Biological* (Springer, Berlin)
42. Z.B. Alfassi, R.E. Huie, P. Neta, J. Phys. Chem. **97**, 28 (1993)
43. I.N. Levine, *Physical Chemistry* (McGraw-Hill, New York, 2011)
44. A. Khazaei, N. Sarmasti, J.Y. Seyf, M. Tavasoli, RSC Adv. **5**, 123 (2015)
45. M.A. Zolfigol, A. Khazaei, N. Sarmasti, J.Y. Seyf, V. Khakyzadeh, A.R. Moosavi-Zare, Appl. Catal, A. **393**, 142 (2014)
46. D.D. Frey, F. Engelhardt, E.M. Greitzer, Res. Eng. Des. **14**, 2 (2003)
47. D.C. Montgomery, *Design and Analysis of Experiments* (Wiley, New York, 1976)
48. M.A. Kulkarni, U.P. Lad, U.V. Desai, S.D. Mitragotri, P.P. Wadgaonkar, C. R. Chimie. **16**, 2 (2013)
49. M. Curini, F. Epifano, S. Chimichi, F. Montanari, M. Nocchetti, O. Rosati, Tetrahedron Lett. **46**, 20 (2005)
50. A. Sinhamahapatra, N. Sutradhar, B. Roy, A. Tarafdar, H.C. Bajaj, A.B. Panda, Appl. Catal. A. **385**, 1 (2010)
51. X. Liu, Z. Ma, J. Xing, H. Liu, J. Magn. Magn. Mater. **270**, 1 (2004)